

# Cooperative relative navigation for multi-UAV systems by exploiting GNSS and peer-to-peer ranging measurements

Jiawen Shen | Shizhuang Wang  | Yawei Zhai  | Xingqun Zhan 

School of Aeronautics and Astronautics, Shanghai Jiao Tong University, Shanghai, People's Republic of China

## Correspondence

Xingqun Zhan, School of Aeronautics and Astronautics, Shanghai Jiao Tong University, No. 800, Dongchuan Road, Shanghai, China.  
Email: xqzhan@sjtu.edu.cn

## Funding information

5G Telecommunication Project in Jiangxi Province: Research on Free Flow Toll Collection Technology Based on 5G+Beidou System, Grant/Award Number: 20193ABC03A006; Key R&D Program Projects in Jiangxi Province: Key Technologies of Intelligent High-speed Application Service Based on Beidou System, Grant/Award Number: 20181ACE50027; Research Achievements Industrialization Foundation of the MoE Research Center on Aerospace Science and Technology

## Abstract

Multiple unmanned aerial vehicle (UAV) systems have attracted extensive research interest for their potential benefits of scalability and flexibility. To keep all the UAVs in the desired formation, the navigation system must continuously provide highly accurate and robust relative positioning results. In open-sky areas, this mission can be achieved using Global Satellite Navigation System (GNSS). However, the performance will be significantly degraded in urban canyons, due to signal blockage or high multipath. In response, we propose a cooperative relative navigation method that exploits peer-to-peer (P2P) ranging measurements to assist GNSS, and introduce cooperative technology to relative navigation. The principle of this approach is integrating multiple observations from multiple sensors and vehicles in the formation, thereby (a) improves navigation accuracy and (b) enhances the robustness against operational scenario changes. Simulations and flight experiments are carried out to validate the proposed algorithm in urban environments, and the results reveal significant accuracy improvement comparing to GNSS only. In addition, multiple sets of sensitivity analyses are performed to address the impact of UAV numbers, formation geometry and accuracy of P2P ranging on navigation performance.

## 1 | INTRODUCTION

In recent years, there has been an increasing interest in multiple unmanned aerial vehicle (UAV) systems because of their immense values. They are expected to be employed for cluster reconnaissance and attack, UAV-based aerial surveillance, ground observation, small packet delivery, and commercial shows [1–4]. Comparing to single UAV, multi-UAV systems can offer significantly enhanced flexibility (adaptability, scalability, and maintainability) and robustness (reliability, survivability, and fault tolerance) [5].

Accurate relative navigation information is the precondition to achieve multi-UAV formation flight [6], especially for formation maintenance [7] and collision avoidance [8]. In open-sky areas, Global Satellite Navigation System (GNSS) can provide the relative position information with high accuracy. In urban areas, however, the navigation performance will be heavily degraded due to the surfaces that block out the signals or generate signal reflections. Signal blockages could reduce the satellite visibility, and signal reflections may lead to heavy

multipath interferences and non-line-of-sight (NLOS) receptions [9–11]. On the other hand, due to the limitations of cost, load, endurance, and size, a UAV cannot simultaneously carry too many high-precise sensors [12]. These issues bring significant challenges to the relative navigation of multi-UAV systems in urban areas.

In the 1970s, Haken proposed the concept of ‘synergy’ and pointed out that ‘ $1 + 1 > 2$ ’ synergy effect can be achieved if the subsystems of a system cooperate with each other around the goal [13]. Cooperative navigation is a technology that utilizes information communication from multiple vehicles. It can effectively solve the aforementioned problems by means of increasing the information redundancy and enhancing the robustness of the navigation system [14]. Communication network allows vehicles to exchange their information with low latency by Bluetooth, ZigBee, or 5G technology [15]. Data fusion combines multiple sources of information including local observations from GNSS receivers and sensors [16].

The concept of cooperative navigation was first proposed in the field of multi-robot systems [17–19], and it has been

This is an open access article under the terms of the Creative Commons Attribution License, which permits use, distribution and reproduction in any medium, provided the original work is properly cited.

© 2020 The Authors. *IET Radar, Sonar & Navigation* published by John Wiley & Sons Ltd on behalf of The Institution of Engineering and Technology.

recently extended to multi-UAV field with a great deal of strategies emerging. Gross et al. proposed a UAV–unmanned ground vehicle cooperative navigation scheme to enhance the navigation performance of the UAV operating in GNSS-challenging environments [20]. And Causa et al. presented a UAV–UAV cooperative strategy where the navigation of the UAV in harsh GNSS conditions is assisted by the UAV flying in open-sky areas [21]. However, most studies about cooperative navigation focused on absolute navigation of one specific agent and failed to put emphasis on relative navigation of multi-UAV systems. As for the relative navigation in a dual- or multi-UAV formation, some studies were carried out and various multi-sensor-relative navigation approaches were proposed. For example, Vision-Based Navigation System [22], Ultraviolet Direction and Ranging [23], and ranging radio [24] are used to offer relative observations for enhancing relative positioning. And Gross et al. designed a high-accuracy relative navigation system by fusing Carrier-Phase Differential Global Positioning System (CP-DGPS), peer-to-peer (P2P) ranging radios, and low-cost inertial measurement unit (IMU) [25]. Xiong et al. investigated the relative navigation performance provided by the fusion of ultra-wideband (UWB) and DGPS [26]. However, these relative navigation schemes only employed the information from two agents rather than all the measurements in the formation. Besides, a few recent research works proposed the cooperative relative navigation schemes for multi-UAV systems [27–29], in which GNSS measurements were not employed. And these schemes paid more attention to formation control than the navigation system itself. To the best of our knowledge, no work has provided a systematic design, analysis, and evaluation about cooperative relative navigation that fully exploits the measurements in a multi-UAV formation.

In response, this study introduces cooperative technology into relative navigation systems for multi-UAV formations by exploiting GNSS observations and P2P ranging measurements. Unlike the existing research works, the proposed algorithm can not only fuse the information from different sensors for relative navigation, but also employ the navigation information from more than two UAVs for cooperation.

GNSS receivers can distinctly output code-phase measurements (i.e., pseudoranges) and carrier-phase measurements (i.e., carriers). Stable carrier-phase observations are often employed to smooth the barcode measurements provided by receivers for achieving higher accuracy. They are available in the situations where high-end receivers are used or the signal quality is favourable (e.g., in open-sky environments). In contrast, in GNSS-challenging environments, unsmoothed pseudoranges (i.e., the raw observations provided by receivers) are usually used for relative navigation due to the limited availability of stable carrier-phase measurements. This situation usually happens when low-cost receivers are utilized in urban dynamic applications. Therefore, pseudoranges are employed here for relative navigation. As for P2P ranging measurement, it is based on one-dimensional range offered by UWB. We consider the poor satellite visibility issue in urban areas. NLOS reception and heavy multipath interference [30] could lead to large measurement

errors, but they are not considered here. In future work, we will develop a cooperative fault detection and exclusion (FDE) framework to account for them.

The rest of this paper is organized as follows. Section 2 describes the measurement models. Section 3 proposes the cooperative relative navigation algorithm and derives the associated covariance. Then, Section 4 focuses on the evaluation and validation of the proposed algorithms by simulations and flight experiments. Finally, Section 5 draws the conclusions and presents some perspectives for future work.

## 2 | MEASUREMENT MODELS

This section describes the models related to a GNSS-based relative navigation algorithm. Section 2.1 provides the GNSS pseudorange double-difference (DD) measurement models, with its error models illustrated in Section 2.2. Then, Section 2.3 introduces the P2P ranging measurements and its error model.

### 2.1 | GNSS pseudorange double difference

For a given receiver  $b$  and a given satellite  $k$ , the pseudorange observation equation is given by [31, 33]

$$\rho_b^k = d_b^k + E_b^k + c(\delta t_b - \delta t^k) + I_b^k + T_b^k + \varepsilon_b^k, \quad (1)$$

where

- The superscript corresponds to individual satellite and the subscript is associated with individual receiver.
- $d$  is the geometrical range between the satellite and the receiver;
- $E$  is the ephemeris error, that is, the difference between the broadcast orbit and the actual value;
- $c$  is the speed of light in vacuum;
- $\delta t_b$  denotes the clock offset of receiver  $b$ ;
- $\delta t^k$  denotes the clock offset of satellite  $k$ ;
- $I$  represents the propagation delay of ionosphere; and
- $T$  represents the propagation delay of troposphere;
- $\varepsilon$  is the pseudorange noise term caused by multipath and receiver noise.

The most significant error sources are shown in Equation (1). For receivers in close proximity, the satellite clock error, satellite ephemeris, ionospheric delay, and tropospheric delay contained in the measurements are approximately equal. As a result, it is possible to eliminate errors that are common to both receivers.

As shown in Figure 1, a single difference (SD) is a combination by differencing the corresponding measurements from two receivers, with which the satellite ephemeris, clock errors, and the propagation errors are eliminated, but the receiver clock-offset term (i.e.,  $\delta t_r - \delta t_b$ ) remains unknown. DD is formed by differencing two SD measurements from different satellites, which removes the receiver clock-offset

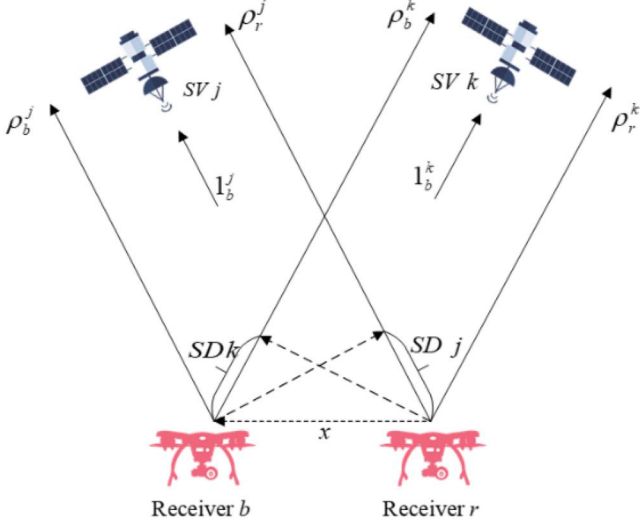


**FIGURE 1** Formation of Global Satellite Navigation System single-difference observations

term [32]. The major exception is multipath and receiver noise since they are uncorrelated between receivers.

The pseudorange DD observation is formed with two separate receivers and two satellites as follows:

$$\rho_{rb}^{jk} \triangleq \rho^{(\hat{j})} = \left( \rho_r^j - \rho_b^j \right) - \left( \rho_r^k - \rho_b^k \right), \quad (2)$$

where subscripts  $r$  and  $b$  refer to the individual receivers; superscripts  $j$  and  $k$  are the individual satellites, and satellite  $k$  is chosen as the reference satellite which is usually the one with the highest elevation angle; and superscript  $(\hat{j})$  denotes the new sequence number of the visible satellites after removing reference satellite  $k$  from the original sequence.

The objective of relative navigation is to estimate the baseline vector, that is, the relative position vector between the two receivers. To relate the DD observation  $\rho^{(\hat{j})}$  with the baseline vector  $\mathbf{x}$  (from receiver  $r$  to receiver  $b$ ), we divided  $\rho^{(\hat{j})}$  into the error-free component  $d_{rb}^{jk}$  and the noise component  $\epsilon_{rb}^{jk}$  as follows [33]:

$$\rho^{(\hat{j})} = d_{rb}^{jk} + \epsilon_{rb}^{jk}. \quad (3)$$

The error-free component  $d_{rb}^{jk}$  is equal to the difference of the baseline vector projections into the LOS vectors from the receiver to two different satellites:

$$d_{rb}^{jk} \triangleq \left( d_r^j - d_b^j \right) - \left( d_r^k - d_b^k \right) = \left[ \mathbf{1}_b^j - \mathbf{1}_b^k \right] \cdot \mathbf{x}, \quad (4)$$

where  $\mathbf{1}_b^j$  is the normalized LOS vector from receiver  $b$  to satellite  $j$ . Therefore,  $d_{rb}^{jk}$  describes the effect of the unknown baseline vector  $\mathbf{x}$ .

The noise component  $\epsilon_{rb}^{jk}$  shows the effect of multipath and receiver noise on the DD measurement:

$$\epsilon_{rb}^{jk} \triangleq \epsilon^{(\hat{j})} = \left( \epsilon_r^j - \epsilon_b^j \right) - \left( \epsilon_r^k - \epsilon_b^k \right). \quad (5)$$

With Equation (4) and (5), Equation (3) can be rewritten as

$$\rho^{(\hat{j})} = \mathbf{1}_b^{(\hat{j})} \cdot \mathbf{x} + \epsilon^{(\hat{j})}, \quad (6)$$

where  $\mathbf{1}_b^{(\hat{j})} = [\mathbf{1}_b^j - \mathbf{1}_b^k]$ , that is, the difference between the LOS vectors for satellite  $j$  and satellite  $k$ .

## 2.2 | Error models of the DD observations

With the DD processing technique illustrated in Section 2.1, most of the error sources in pseudoranges have been eliminated, leaving the DD observation errors dominated by multipath and receiver noise.

Unsmoothed pseudoranges (i.e., without carrier smoothing) are employed here. The nominal error models for the multipath and receiver noise in the SD measurement corresponding to satellite  $j$  ( $SD^j = \rho_r^j - \rho_b^j$ ) can be modelled as [34]

$$\sigma_{\text{MP,SD}}^j = \sqrt{2} \times \sigma_{\text{MP}}^j \quad (7)$$

$$\sigma_{\text{RN,SD}}^j = \sqrt{2} \times \sigma_{\text{RN}}^j, \quad (8)$$

where  $\sigma_{\text{MP}}^j$  is the standard deviation of multipath and  $\sigma_{\text{RN}}^j$  is the standard deviation of receiver noise; both are in metres.

Then the SD measurement error diagonal covariance matrix  $\mathbf{C}_{\text{SD}}$  can be determined by combining the effects of multipath and receiver noise as follows [35]:

$$\mathbf{C}_{\text{SD}}(j,j) = \left( \sigma_{\text{MP}}^j \right)^2 + \left( \sigma_{\text{RN}}^j \right)^2, j = 1, 2, \dots, N_S, \quad (9)$$

where  $N_S$  is the number of the visible satellites to the receiver.

Based on Equation (2), the DD measurement error covariance matrix  $\mathbf{C}_{\text{DD}}$  can be computed as [33]

$$\mathbf{C}_{\text{DD}} = \mathbf{B} \cdot \mathbf{C}_{\text{SD}} \cdot \mathbf{B}^T, \quad (10)$$

where  $\mathbf{B}$  denotes the  $(N_S-1)$ -by- $N_S$  transformation matrix from SD to DD, which is given by

$$\mathbf{B} = \begin{bmatrix} 1 & 0 & 0 & -1 & 0 & 0 & 0 \\ 0 & 1 & 0 & -1 & 0 & 0 & 0 \\ 0 & 0 & \ddots & \vdots & 0 & 0 & 0 \\ 0 & 0 & 0 & -1 & \ddots & 1 & 0 \\ 0 & 0 & 0 & -1 & 0 & 0 & 1 \end{bmatrix}, \quad (11)$$

where: all the entries in the  $k$ -th column (corresponding to the reference satellite  $k$ ) are equal to  $-1$ .

## 2.3 | P2P ranging model

Modules such as UWB and vision sensor can provide relative range measurement from peer to peer directly. UWB can provide one-dimensional range, while vision sensor can provide three-dimensional range. The P2P ranging measurement model is based on one-dimensional range offered by UWB here. The measurement component can be divided into the baseline component and the error component  $\omega_{rb}$  as follows:

$$m_{rb} = \mathbf{x} + \omega_{rb} = \mathbf{1}_x \cdot \mathbf{x} + \omega_{rb} \quad (12)$$

where  $m_{rb}$  is the P2P ranging measurement between two UAVs,  $\mathbf{x}$  denotes the length of vector  $\mathbf{x}$ , and  $\mathbf{1}_x$  is the normalized vector from UAV  $r$  to UAV ( $b$ )

The noise error can be modelled as a zero-mean Gaussian distribution with standard deviation of  $\sigma_{\text{uwb}}$ .

## 3 | PROPOSED COOPERATIVE RELATIVE NAVIGATION ALGORITHM

This section describes a GNSS-based relative navigation algorithm aided by P2P ranging measurements. Section 3.1 presents the equations to obtain the baseline between two UAVs based on DD observations and P2P ranging. Next, the mathematical model of the relative cooperative navigation algorithm is derived in Section 3.2. Then, Section 3.3 introduces the model of the related covariance matrix.

### 3.1 | Relative navigation between dual UAVs based on DD and P2P ranging measurement

Assuming that there are  $N_S$  satellites visible to both receivers on UAV  $b$  and  $r$ , and the one with the highest elevation angle is chosen as the reference satellite. Therefore, the measurements of  $N_S$  satellites form  $(N_S - 1)$  DD observations. In the meantime, the P2P ranging measurement is provided for the two UAVs. To combine the P2P ranging measurement with the DD observations, the combination and extension of Equations (6) and (12) are expressed as follows:

$$\begin{bmatrix} \rho^{(1)} \\ \rho^{(2)} \\ \vdots \\ \rho^{(N_S-1)} \\ m_{rb} \end{bmatrix} = \begin{bmatrix} 1_b^{(1)} \\ 1_b^{(2)} \\ \vdots \\ 1_b^{(N_S-1)} \\ \mathbf{1}_x \end{bmatrix} \mathbf{x} + \begin{bmatrix} \varepsilon^{(1)} \\ \varepsilon^{(2)} \\ \vdots \\ \varepsilon^{(N_S-1)} \\ \omega_{rb} \end{bmatrix}. \quad (13)$$

Equation (13) can be rewritten as

$$\boldsymbol{\rho}_{rb} = \mathbf{A} \cdot \mathbf{x} + \boldsymbol{r}_b \quad (14)$$

The baseline vector  $\mathbf{x}$  can be estimated by weighted least-squares (WLS). The update for  $\Delta \hat{\mathbf{x}}$  at each iteration is given by

$$\Delta \hat{\mathbf{x}} = \left( \mathbf{A}^T \mathbf{W}_D \mathbf{A} \right)^{-1} \mathbf{A}^T \mathbf{W}_D \cdot \Delta \boldsymbol{\rho}_{rb} \quad (15)$$

where  $\Delta \boldsymbol{\rho}_{rb}$  is composed of two parts: one is the vector of DD observations minus the expected DD values based on the matrix  $\mathbf{A}$  and the baseline solution given by the previous iteration, the other is the difference of P2P ranging measurement and the expected relative ranging value based on the solution of previous iteration. In this equation, the observations are weighted by the diagonal matrix  $\mathbf{W}_D$ .

The weighting matrix  $\mathbf{W}_D$  is determined by the covariance matrix  $\mathbf{C}_{DD}$  and the covariance of the P2P ranging measurement. Let the weight of the  $\hat{j}$ th DD measurement be equal to the reciprocal of the associated covariance, as shown in the following equation:

$$\mathbf{W}_D(\hat{j}, \hat{j}) = (\mathbf{C}_{DD}(\hat{j}, \hat{j}))^{-1}, \hat{j} = 1, 2, \dots, N_S - 1. \quad (16)$$

The P2P ranging measurement part of weighting matrix  $\mathbf{W}_D$  is equal to the reciprocal of the P2P ranging measurement associated variance:

$$\mathbf{W}_D(N_S, N_S) = (\sigma_{\text{uwb}}^2)^{-1} \quad (17)$$

Then, the covariance matrix of all the observations, that is,  $\mathbf{C}_{OB}$ , is as follows:

$$\mathbf{C}_{OB} = \begin{bmatrix} \mathbf{C}_{DD} & 0 \\ 0 & \sigma_{\text{uwb}}^2 \end{bmatrix} \quad (18)$$

### 3.2 | Multi-UAV cooperative relative navigation algorithm

Assuming that there are  $N$  UAVs in the formation, the observations and communication structure among the UAVs are shown as in Figure 2. The baseline estimates  $\mathbf{e}$  between each two UAVs can be provided by the solutions illustrated in Section 3.1.

The UAV with the most visible satellites in the formation is chosen as the base, which is identified as UAV  $b$ . Then, a local East, North, Up (ENU) frame is established with UAV  $b$  as the

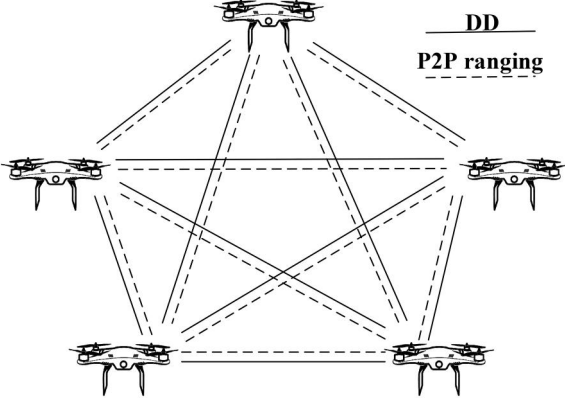


FIGURE 2 Observations and communication structure in the multi-unmanned aerial vehicle system

origin. The relative positions of other UAVs can be obtained by the baseline vector estimations about UAV  $b$ .

It is worth mentioning that in practice, the visible satellites may be not sufficient to derive an absolute position estimate. However, the relative navigation process may still be executed in this case. And the absence of absolute position referencing will influence the proposed relative navigation scheme by disabling the following process: (a) the calculation of the transformation matrix from the Earth-centred Earth-fixed (ECEF) frame to the local ENU frame; and (b) the determination of the LOS vectors from the receiver to the satellite. Fortunately, both (a) and (b) are not sensitive to the absolute position, and an absolute position estimate with 10-km accuracy is generally enough for them.

It should also be noted that the relative navigation between two UAVs may fail due to limited visible satellites. For example, it is possible that only two satellites are both visible to UAV  $i$  and UAV  $r$ , that is, only one DD measurement can be formed. In this case, the DD observation and the P2P ranging measurement remain as follows:

$$\begin{bmatrix} \rho_{ir}^{(1)} \\ m_{ir} \end{bmatrix} = \begin{bmatrix} 1_r^{(1)} \\ 1_{x,ir} \end{bmatrix} \mathbf{x}_{ir} + \begin{bmatrix} \boldsymbol{\epsilon}^{(1)} \\ \boldsymbol{\omega}_{ir} \end{bmatrix} \quad (19)$$

where  $\rho_{ir}^{(1)}$  is the DD observation,  $1_r^{(1)}$  is the difference of the unit vectors from UAV  $r$  to satellite 1 and the reference satellite,  $1_{x,ir}$  is the normalized vector from UAV  $i$  to UAV  $r$ , and  $\mathbf{x}_{ir}$  is the baseline vector from UAV  $i$  to UAV  $r$ , which is related to the direction vectors from UAV 1 to UAV  $i$  and UAV  $r$ , respectively, that is,  $\mathbf{x}_{ir} = \mathbf{x}_{br} - \mathbf{x}_{bi}$ . Thus, with the estimated baseline vector, Equation (19) can be rewritten as

$$\begin{bmatrix} \rho_{ir}^{(1)} - 1_r^{(1)} \cdot \mathbf{e}_{br} \\ m_{ir} - 1_{x,ir} \cdot \mathbf{e}_{br} \end{bmatrix} = \begin{bmatrix} -1_r^{(1)} \\ -1_{x,ir} \end{bmatrix} \mathbf{x}_{bi} + \begin{bmatrix} \boldsymbol{\epsilon}^{(1)} \\ \boldsymbol{\omega}_{ir} \end{bmatrix}, \quad (20)$$

where  $\mathbf{e}_{br}$  is the estimation solved in Equation (14), and  $1_{x,ir}$  can be calculated by  $1_{x,ir} = \frac{\mathbf{e}_{br} - \mathbf{x}_{bi}}{|\mathbf{e}_{br} - \mathbf{x}_{bi}|}$ .

As the fusion equation of the DD observation and the P2P ranging measurement, Equation (20) can be rewritten as

$$\mathbf{f}_{ir} = \mathbf{H}_{ir} \cdot \mathbf{x}_{bi} + \boldsymbol{\nu}_{ir} \quad (21)$$

Figure 3 shows the procedures for the algorithm based on DD and P2P ranging measurements between dual UAVs. The data acquisition unit is composed of the GNSS receivers and P2P ranging modules (e.g., UWB) carried on the UAVs. And the vehicle-to-vehicle (V2V) unit serves as the information communication among the UAVs.

Figure 4 presents the flowchart of the proposed cooperative relative navigation algorithm scheme based on the estimations solved by dual UAVs. This algorithm will be illustrated in detail as follows.

First, the baseline vector between UAVs  $b$  and  $i$  can be given by

$$\begin{bmatrix} \mathbf{e}_{bi} \\ \mathbf{e}_{bu} + \mathbf{e}_{ui} \\ \vdots \\ \frac{\mathbf{e}_{bN} + \mathbf{e}_{Ni}}{m_{bi}} \\ \frac{\mathbf{f}_{ir}}{m_{bi}} \end{bmatrix} = \begin{bmatrix} \mathbf{I}_{3 \times 3} \\ \mathbf{I}_{3 \times 3} \\ \vdots \\ \mathbf{I}_{3 \times 3} \\ \mathbf{H}_{ir} \\ 1_{x,bi} \end{bmatrix} \mathbf{x}_{bi} + \begin{bmatrix} \hat{\boldsymbol{\epsilon}}_{bi} \\ \hat{\boldsymbol{\epsilon}}_{bu} + \hat{\boldsymbol{\epsilon}}_{ui} \\ \vdots \\ \hat{\boldsymbol{\epsilon}}_{bN} + \hat{\boldsymbol{\epsilon}}_{Ni} \\ \frac{\boldsymbol{\epsilon}_{ir}}{\omega_{bi}} \end{bmatrix}, \quad (22)$$

where  $\mathbf{e}$  is the baseline estimate in previous step;  $\mathbf{I}_{3 \times 3}$  is a 3-by-3 identity matrix;  $\hat{\boldsymbol{\epsilon}}$  is the 3-by-3 error matrix of the baseline estimation.

Equation (22) can be rewritten as:

$$\mathbf{y}_{bi} = \mathbf{G} \cdot \mathbf{x}_{bi} + \boldsymbol{\nu}_{bi} \quad (23)$$

The baseline vector  $\mathbf{x}_{bi}$  can be estimated by WLS. The update for  $\Delta \hat{\mathbf{x}}_{bi}$  at each iteration is given by

$$\Delta \hat{\mathbf{x}}_{bi} = \left( \mathbf{G}^T \mathbf{W}_M \mathbf{G} \right)^{-1} \mathbf{G}^T \mathbf{W}_M \cdot \Delta \mathbf{y}_{bi} \quad (24)$$

where  $\Delta \mathbf{y}_{bi}$  is the vector of observations in Equation (23) minus the expected values. The initial value of the baseline vector is given by the result of the solution in Section 3.2, and the observations, that is, the estimated baseline vector  $\mathbf{e}$ , will be updated by the solution  $\mathbf{x}$ . The observations are weighted by the diagonal matrix  $\mathbf{W}_M$ , which is determined by the associated covariance:

$$\mathbf{W}_M(l, l) = (\mathbf{C}_M(l, l))^{-1} \quad (25)$$

The covariance matrix  $\mathbf{C}_M$  is a diagonal matrix decided by the covariance matrix of each observation:



### 3.3 | Covariance estimation

The covariance matrix of the observation  $\mathbf{e}_{ui}$  can be modelled as

$$\mathbf{C}_{\mathbf{e}(ui)} = \mathbf{S}_{D,ui} \mathbf{C}_{\text{OB},ui} \mathbf{S}_{D,ui}^T \quad (32)$$

where matrix  $\mathbf{S}_{D,ui} = (\mathbf{A}_{ui}^T \mathbf{W}_{D,ui} \mathbf{A}_{ui})^{-1} \mathbf{A}_{ui}^T \mathbf{W}_{D,ui}$  from the solution in Equation (15).

As for  $\mathbf{e}_{bu} + \mathbf{e}_{ui}$ , which is the sum of two observations  $\mathbf{e}$  and  $\mathbf{e}_{bi} - \mathbf{e}_{bu}$ , which is the difference of two observations, the covariance can be given by

$$\mathbf{C}_{\mathbf{e}(bu+ui)} = \mathbf{C}_{\mathbf{e}(bu)} + \mathbf{C}_{\mathbf{e}(ui)} + 2 \times \mathbf{C}_{\mathbf{e}(bu,ui)} \quad (33)$$

$$\mathbf{C}_{\mathbf{e}(bi-bu)} = \mathbf{C}_{\mathbf{e}(bi)} + \mathbf{C}_{\mathbf{e}(bu)} - 2 \times \mathbf{C}_{\mathbf{e}(bi,bu)} \quad (34)$$

where  $\mathbf{C}_{\mathbf{e}(bu,ui)}$  represents the covariance matrix between  $\mathbf{e}_{bu}$  and  $\mathbf{e}_{ui}$ . This is formed by the observations of two estimations, that is,  $\mathbf{C}_{\mathbf{e}(bu,ui)} = \mathbf{S}_{D,bu} \mathbf{C}_{\text{OB}(bu,ui)} \mathbf{S}_{D,ui}^T$ , with  $\mathbf{C}_{\text{OB}(bu,ui)}$  as

$$\mathbf{C}_{\text{OB}(bu,ui)} = \begin{bmatrix} \mathbf{C}_{\text{DD}(bu,ui)} & 0 \\ 0 & 0 \end{bmatrix} \quad (35)$$

where the  $(n-1)$ -by-  $(m-1)$  matrix  $\mathbf{C}_{\text{DD}(bu,ui)}$  is as follows:

$$\mathbf{C}_{\text{DD}(bu,ui)}(p, q) = \begin{cases} (\sigma_{\text{user},u}^k)^2, & p \neq q \\ (\sigma_{\text{user},u}^k)^2 + (\sigma_{\text{user},u}^p)^2, & p = q \end{cases} \quad (36)$$

where  $n$  is the number of the common-view satellites to UAV  $b$  and  $u$ , while  $m$  is the number of the common-view satellites to UAV  $u$  and  $i$ ; therefore, the number of DD observations are  $(n-1)$  and  $(m-1)$ , respectively; subscript  $k$  denotes the reference satellite and  $\sigma_{\text{user},u}^p$  is the user error of receiver  $u$  to satellite  $p$ , which can be given by the standard deviation of multipath and receiver noise [34]:

$$\sigma_{\text{user},u}^p = \sqrt{(\sigma_{\text{MP}}^p)^2 + (\sigma_{\text{RN}}^p)^2} \quad (37)$$

Therefore, the covariance estimation of the baseline will be updated by

$$\mathbf{C}_{\mathbf{e}(bu)} = \mathbf{S}_{M,bu} \mathbf{C}_{M,bu} \mathbf{S}_{M,bu}^T \quad (38)$$

where matrix  $\mathbf{S}_{M,bu} = (\mathbf{G}_{bu}^T \mathbf{W}_{M,bu} \mathbf{G}_{bu})^{-1} \mathbf{G}_{bu}^T \mathbf{W}_{M,bu}$  from the solution in Equation (24), and  $\mathbf{C}_{M,bu}$  comes from Equation (26).

**TABLE 1** Descriptions for the methods compared

No.	Measurements	Cooperative or not?	Label
1	Pseudorange	×	DD
2	Pseudorange P2P ranging	×	DD&P2P
3	Pseudorange P2P ranging	√	CRN

Abbreviations: CRN, Cooperative Relative Navigation; DD, double difference; P2P, peer-to-peer.

**TABLE 2** Standard deviations of the receiver-dependent range measurements errors in a single-frequency receiver [36]

Contributing source	Standard deviation (m)
Receiver noise	0.3
Multipath	0.5

## 4 | EXPERIMENTS AND RESULTS

In this section, simulations are carried out to evaluate the performance of the relative navigation system. In Section 4.1, simulation configurations are presented, and the simulations are performed in Section 4.2. The sensitivity analyses are carried out in Section 4.3.

### 4.1 | Simulation configurations

A MATLAB-based simulation platform for a 5-UAV system relative navigation performance evaluation is established. The duration of simulation is 1000 s. Table 1 shows the descriptions of the three simulated methods which represent various configurations (regarding measurements and cooperative option) with single-frequency receivers. The standard deviations of the receiver-dependent range measurements errors (i.e., receiver noise and multipath) are given in Table 2. Please note, the large measurement errors caused by heavy multipath and NLOS reception are not considered here. Indeed, they should be regarded as faults and will be addressed by a cooperative FDE scheme in the future work. As for the P2P ranging measurement obtained by UWB modules, the standard deviation  $\sigma_{\text{uwb}}$  is set to 0.1 m according to the datasheet of a well-known UWB module, that is, DWM 1000.

Figure 5 presents the skyplot of the satellites used in the following process. Additionally, the satellites with the highest elevation angle in each constellation were chosen as the reference satellites, that is, G27 for Global Positioning System (GPS) and C07 for Beidou. To simulate urban canyon, two walls are set both on the west side and the east side of the multi-UAV formation as shown in Figure 6, where the blue dots indicate the UAVs and the grey indicates the walls. The UAVs are numbered from high to low in height. In this

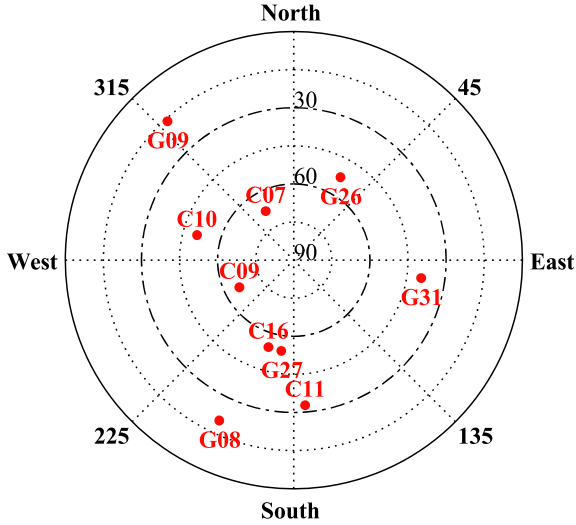


FIGURE 5 Skyplot of the satellites in use (G-GPS, C-Beidou)

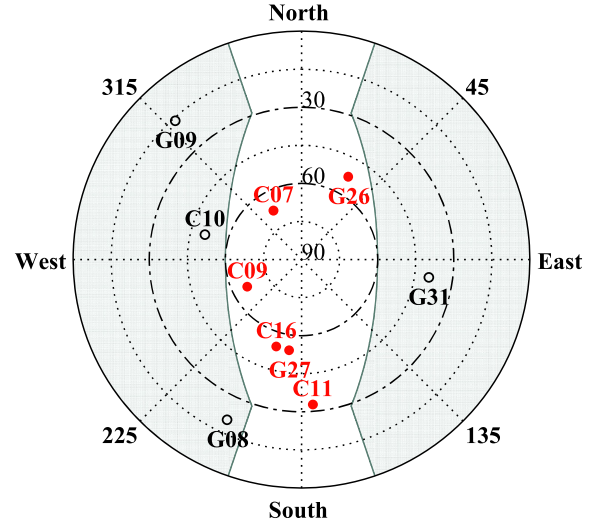


FIGURE 7 Skyplot of the satellites in urban canyon (G-GPS, C-Beidou)

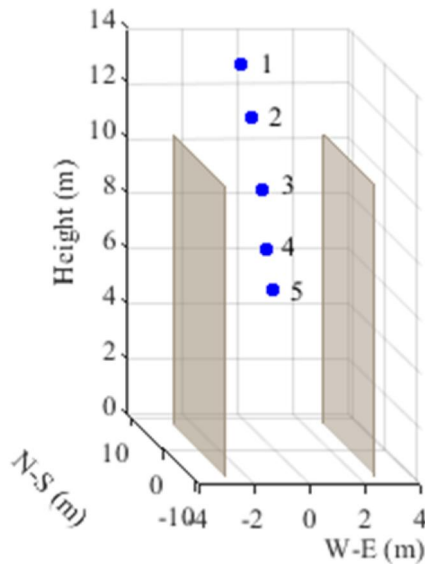


FIGURE 6 Multi-unmanned aerial vehicle formation in urban canyon

circumstance, the condition of available satellites for the UAV 5 is shown in Figure 7, where red dots represent the visible satellites while black points represent the invisible ones which are blocked by the grey shadings.

Table 3 shows the list of the visible satellites for each UAV in the formation after the urban canyon is set. The scenarios can be described as open sky, middle urban, and deep urban [37].

## 4.2 | Simulation for performance evaluation

First, we analyse the accuracy of relative navigation performance by the comparing the results of the DD method and the DD&P2P method. Both of them are based on the information communicated between dual UAVs. Figure 8(a) presents the relative positioning errors of the baseline from UAV 1 to UAV 2

(in open sky). The histograms show that, comparing to the DD approach, the algorithm with P2P ranging measurement improves the accuracy by 23.42%, from 2.22 to 1.70 m. On the other hand, Figure 8(b) suggests the relative positioning errors of the baseline from UAV 1 to UAV 5 (in deep urban). It shows that P2P ranging measurement helps improve the accuracy of the baseline significantly in urban canyon, with the value reduced by 81.77%, from about 14.15 to 2.58 m. The comparisons are summarized in Table 4. The results suggest that the overall relative navigation performance will be severely degraded due to limited satellite visibility and poor measurement accuracy in urban environment. Additionally, the performance can be enormously improved by employing P2P ranging measurements to pseudorange DD, especially in GNSS challenging situations.

Then, we compare the performance with and without information cooperated among multiple UAVs. As seen from Figure 9(a), the CRN algorithm improves the accuracy from 1.70 to 1.02 m (about 40.00% degraded) by making full use of the information among the system rather than between the dual UAVs. For the baseline from UAV 1 to UAV 5 as shown in Figure 9(b), the accuracy is improved from about 2.58 to 1.76 m (about 31.78% degraded) through the CRN algorithm. The comparison results are summarized in Table 5. It is indicated that the relative navigation performance can be significantly improved by cooperating the information of multiple UAVs. Therefore, cooperation is highly desired for multi-UAV systems, especially in urban navigation applications.

In addition, Figure 10 provides a direct view of the performance comparison among all the methods in order to quantitatively reveal the impacts of various factors on the navigation performance. Accuracy is presented in the form of cumulative distribution function (CDF). CDF specifies the probability or normalized frequency that a variable  $X$  takes a value less than or equal to a given value  $x$ . It shows that employing P2P ranging measurement can improve the traditional DD method dramatically, especially in the up direction,

**TABLE 3** The visible satellites for each UAV in the formation

Constellation	PRN	UAV 1	UAV 2	UAV 3	UAV 4	UAV 5
G	08	✓	✓	×	×	×
	09	✓	✓	×	×	×
	26	✓	✓	✓	✓	✓
	27	✓	✓	✓	✓	✓
	31	✓	✓	✓	×	×
C	07	✓	✓	✓	✓	✓
	09	✓	✓	✓	✓	✓
	10	✓	✓	✓	×	×
	11	✓	✓	✓	✓	✓
	16	✓	✓	✓	✓	✓
Total number		10	10	8	6	6
Scenarios		Open sky	Open sky	Middle urban	Deep urban	Deep urban

Note. G – GPS, C – Beidou.

Abbreviations: PRN, Pseudo-Random Noise; UAV, unmanned aerial vehicle.

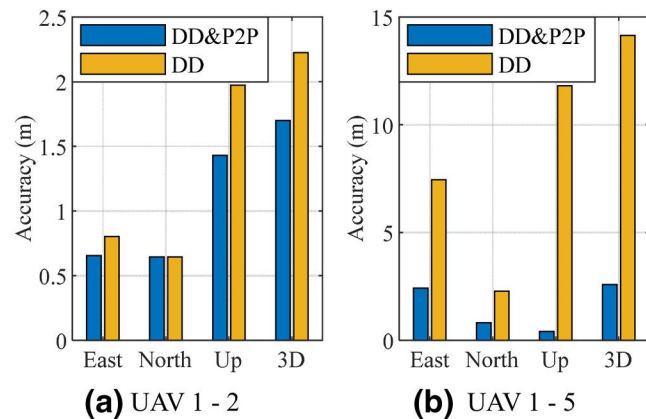


**FIGURE 8** Accuracy of the baseline ([a] from UAV 1 to UAV 2 and [b] from UAV 1 to UAV 5) comparison between the two relative navigation methods with and without peer-to-peer ranging

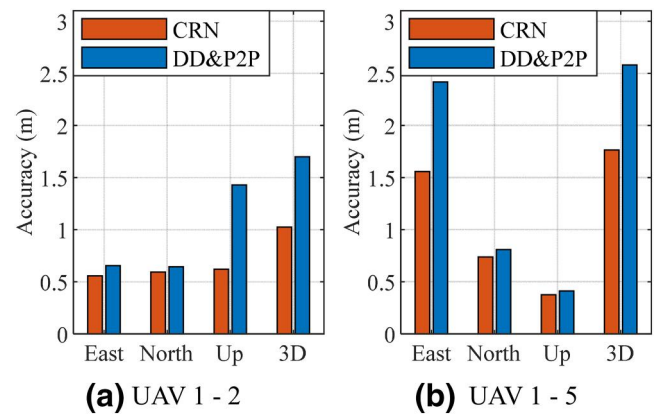


**FIGURE 9** Accuracy of the baseline ([a] from UAV 1 to UAV 2 and [b] from UAV 1 to UAV 5) comparison between the two relative navigation methods with and without cooperation

**TABLE 4** The comparison between the relative performance

Baseline	Direction	Accuracy (m)		Improvement (m)	Percent
		DD	DD&P2P		
UAV 1-2 open sky	E	0.80	0.66	0.14	17.50%
	N	0.65	0.64	0.01	1.54%
	U	1.97	1.40	0.57	28.93%
	3D	2.22	1.70	0.52	23.42%
UAV 1-5 deep urban	E	7.45	2.42	5.03	67.52%
	N	2.28	0.81	1.47	64.47%
	U	11.81	0.41	11.4	96.53%
	3D	14.15	2.58	11.57	81.77%

Abbreviations: DD, double difference; P2P, peer-to-peer; UAV, unmanned aerial vehicle.

Baseline	Direction	Accuracy(m)		Improvement (m)	Percent
		DD&P2P	CRN		
UAV 1–2 open sky	E	0.66	0.55	0.11	6.67%
	N	0.64	0.59	0.05	7.81%
	U	1.43	0.62	0.81	56.64%
	3D	1.70	1.02	0.68	40.00%
UAV 1–5 deep urban	E	2.42	1.56	0.86	35.54%
	N	0.80	0.74	0.06	7.50%
	U	0.40	0.38	0.02	5.00%
	3D	2.58	1.76	0.82	31.78%

Abbreviations: CRN, Cooperative Relative Navigation; DD, double difference; E, east; N, north; P2P, peer-to-peer; U, up; UAV, unmanned aerial vehicle.

**TABLE 5** The comparison between the relative performance

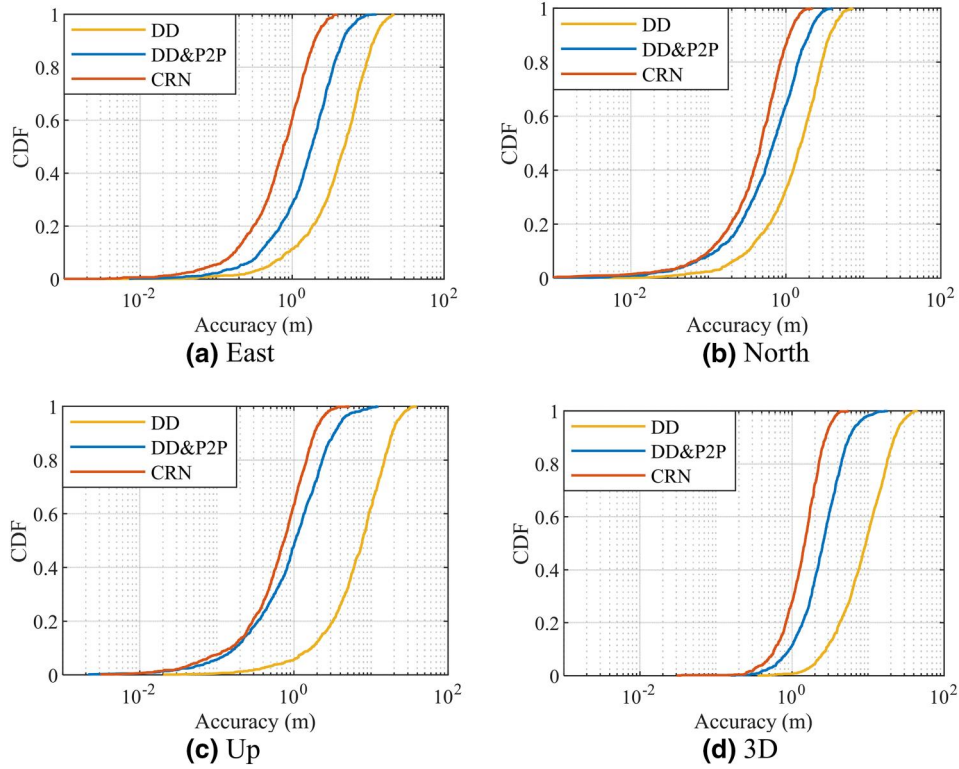


**FIGURE 10** A comprehensive performance comparison among the three methods

followed by the improvement in the east and north. Besides, cooperative relative navigation technology can further the improvement, especially in the north and up directions.

To sum up, it is necessary for applications of multi-UAV formation in urban environment to solve the relative navigation issues. It is proved that employing P2P ranging measurements to the pseudorange DD method can preliminarily improve the accuracy. Additionally, cooperative navigation algorithm can reduce the relative position errors further. Moreover, from this analysis, it is apparent that P2P ranging measurements can offer more benefit in poor environmental conditions.

In order to validate the covariance model, we compare the root of the calculated covariance, that is, SIGMA, with the

statistical standard deviation. Figure 11 presents the statistical and estimated error standard deviations, with (a) representing the middle urban environment and (b) representing the deep urban environment. The results suggest that the baseline can be estimated with satisfactory accuracy by using the proposed algorithm, and they also prove the feasibility of the covariance estimation methodology.

### 4.3 | Sensitivity analysis

To reveal the impacts of the scale of the multi-UAV formation, the formation geometry, and the accuracy of the P2P ranging

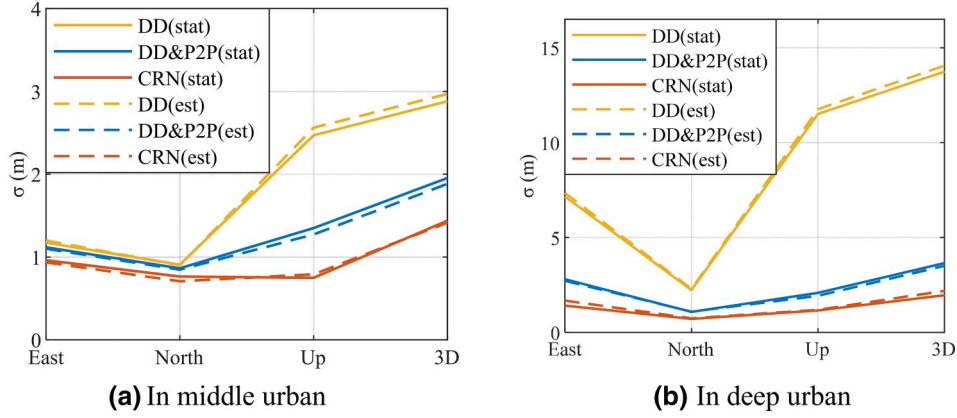


FIGURE 11 The statistical (solid lines) and estimated (dashed lines) error standard deviations

TABLE 6 Simulation configurations in various scenarios

Case no.	Number of UAVs	Formation geometry	UWB accuracy (m)	Urban environment
1	5	E	0.1	×
2		N		
3		U		
4	5	U	0.01	×
5			0.05	
6			0.1	
7			0.5	
8			1.0	
9			2.0	
10			2.5	
11			3.0	
12	3	All	0.1	√
13	5			
14	7			
15	10			
16	15			

Abbreviations: E, east; N, north; U, up; UAV, unmanned aerial vehicle; UWB, ultra-wideband.

module, we conduct the following sensitivity analysis. The 16 scenarios listed in Table 6 are simulated to perform this sensitivity analysis. For each scenario, we conduct Monte-Carlo simulations to generate 1000 random scenarios, which are used to statistically determine the error standard deviations. Although the formation geometry or the formation scale is changed as required, the position of the highest UAV in the formation is fixed among all the cases, which is set as the origin of the local ENU frame. The scale of multi-UAV formation can be distinguished by the number of the UAVs. The formation geometry in the local ENU frame can be classified into the difference of one direction with the other two directions fixed. For example, all the UAVs are different in U direction while they have the same coordinates in E and N directions.

Besides, ‘All’ in Table 6 means that the formation geometry is not fixed in any directions.

Figure 12 shows the impact of formation geometry by the three cases, which are different in E, N, and U directions, respectively. To make the analysis clear, urban environment is not considered here. It shows that the original difference in one specific direction impacts the improvement in this direction achieved by the DD&P2P and CRN algorithms.

Figure 13 shows the influence of the accuracy of P2P ranging module UWB among the cases listed in Table 6. In comparison with the results of DD, both the performance of the DD&P2P and CRN methods will be degraded with the accuracy of P2P ranging measurements getting poorer as shown by Figure 14. When the error of P2P ranging is larger

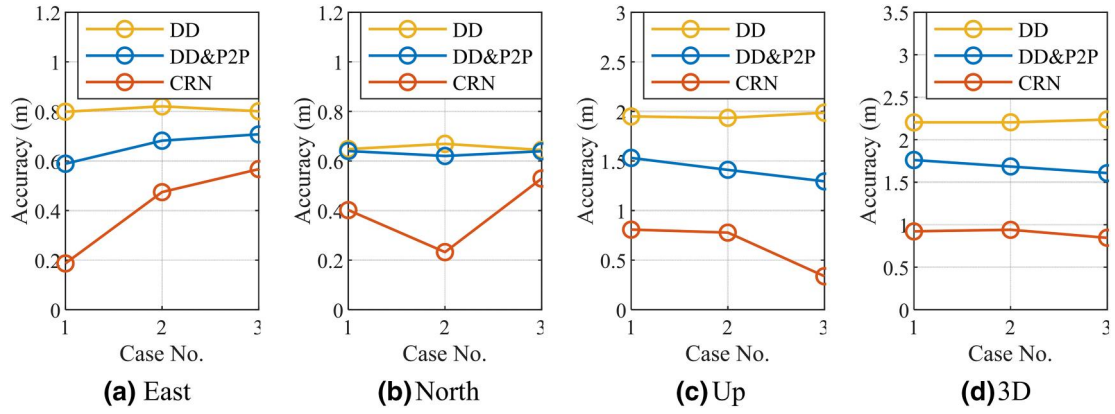


FIGURE 12 The impact of formation geometry

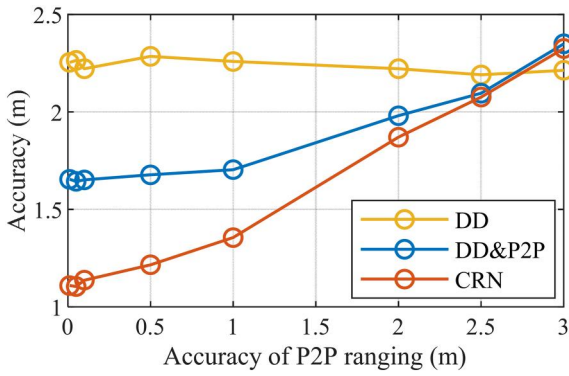


FIGURE 13 The impact of the peer-to-peer ranging accuracy

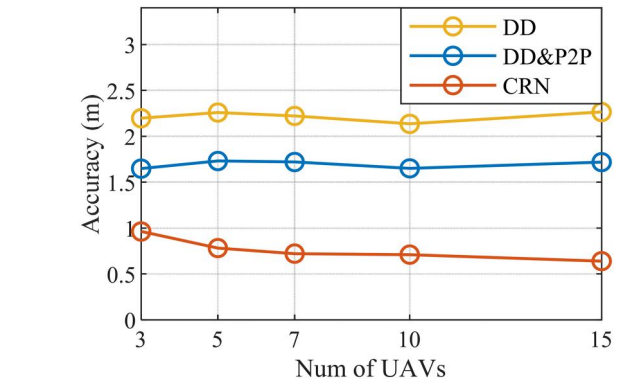


FIGURE 15 The impact of the formation scale

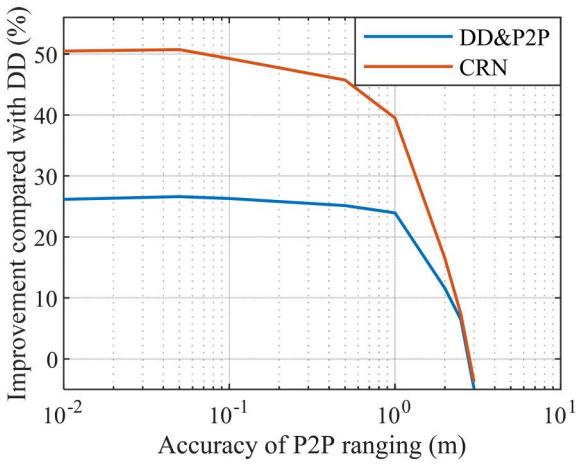


FIGURE 14 Improvement achieved by cooperation with different accuracy of peer-to-peer ranging

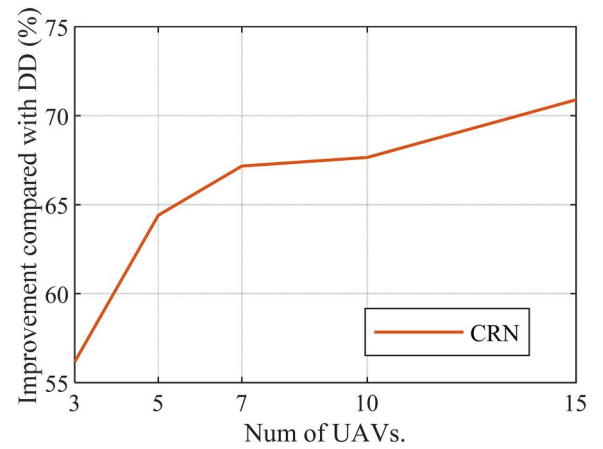


FIGURE 16 Improvement achieved by cooperation in different multi-unmanned aerial vehicle formation scales

than the one of DD, P2P ranging measurement will bring negative influence rather than positive effect. This kind of error is considered as fault, which should be excluded in future work.

The influence of the formation scale on the improvement achieved by the proposed cooperative relative navigation

algorithm is suggested in Figures 15 and 16. To accomplish the proposed cooperative relative navigation system, the formation should include at least three UAVs. Comparing the results of the CRN method to the traditional DD, it is revealed that the larger the scale is, the better the performance will be accomplished by cooperation among the UAVs.

#### 4.4 | Flight test and experimental results

The objective of flight experiments is to validate the proposed algorithm with real data. A test platform is established based on three quadcopters, which can represent the minimum scale of a multi-UAV system and can therefore be used for algorithm validation. As shown in Figure 16, the relative navigation performance will be improved more when the number of UAVs increases. And we will demonstrate the algorithm behaviours with more UAVs in our future work. As shown in Figure 17, each UAV is equipped with several devices for data collection. Raw GNSS measurements (i.e., pseudoranges) are acquired by ublox F9P, a lightweight DFMC GNSS receiver. As an open-source GNSS software [38], Real-time kinematic (RTK) records and stores the data on the on-board computer (i.e., Raspberry Pi 3B+). The network RTK subscription service, that is, FindCM provided by Qianxun SI [39], is utilized to compute the reference position solutions of the UAVs. The P2P ranging measurements are offered by UWB DWM 1000 modules.

Before the flight experiment, we have evaluated the ranging accuracy of this module, and the result suggests that a root-mean-square (RMS) accuracy of about 0.065–0.15 m is achieved when the actual distance ranges from 0.1 to 10 m. This basically verifies the value (i.e., 0.1 m) given in the data-sheet of DWM 1000. However, the UWB range accuracy may be degraded by the obstacles in the surroundings. To avoid this negative effect, we pre-design the attitude of the UAVs to make sure that the UWB modules are also directly visible to each other without any obstacle in their LOS.

The fault caused by NLOS and multipath interference is not taken into consideration here, and it will be discussed in future work. To obtain real data and avoid such faults, the flight experiment was carried out in the campus as shown in Figure 18, where many satellite signals were available and favourable GNSS positioning performance was achieved. Specifically, for safety concerns, high difference was set among the three vehicles. Therefore, the highest vehicle is named UAV 01, and the lowest one is named UAV 03.

To simulate an urban environment, part of visible satellites of UAV 03 was blocked in data processing with only four GPS satellites left. At the same time, there were only eight satellites visible to both UAV 01 and UAV 02. In this way, the scenario can represent the typical satellite visibility in urban areas. Figure 19 shows the comparison of the relative positioning solutions between UAV 01 to UAV 03 computed by DD method and RTK, which indicates the availability of the collected data. The sensitivity analysis over formation geometry is conducted in the simulation part, and this analysis is not repeated in the experiment. Therefore, it is acceptable that the formation geometry is time-varying (as shown in Figure 19) in the flight experiment.

The relative positioning errors are reported with respect to the reference values determined by the RTK technique. By comparing DD&P2P with DD, it can be seen in Figure 20 that P2P ranging measurements can effectively improve the relative positioning solutions. It is observed that the estimation errors



FIGURE 17 Experimental unmanned aerial vehicle system



FIGURE 18 Flight experiment in campus with three unmanned aerial vehicles

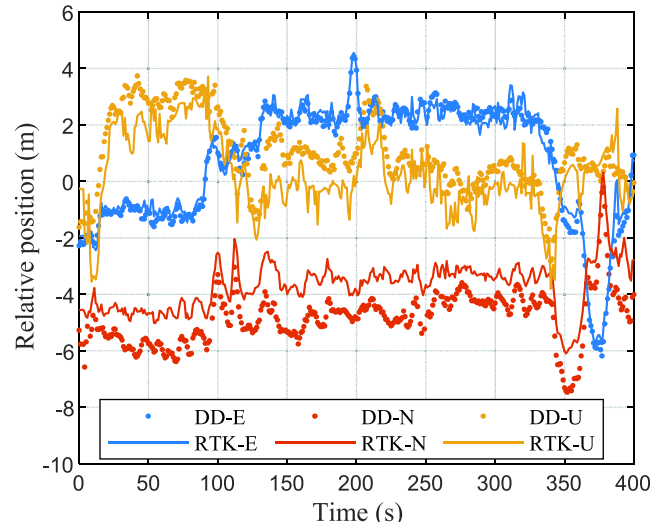


FIGURE 19 The relative positioning results by RTK and double difference. RTK, Real-time kinematic

are not zero-mean, especially in the North and Up directions. This is caused by the pseudorange bias in the low-elevation satellite. This measurement bias may be caused by multipath effects and can directly lead to the bias in the baseline estimate.

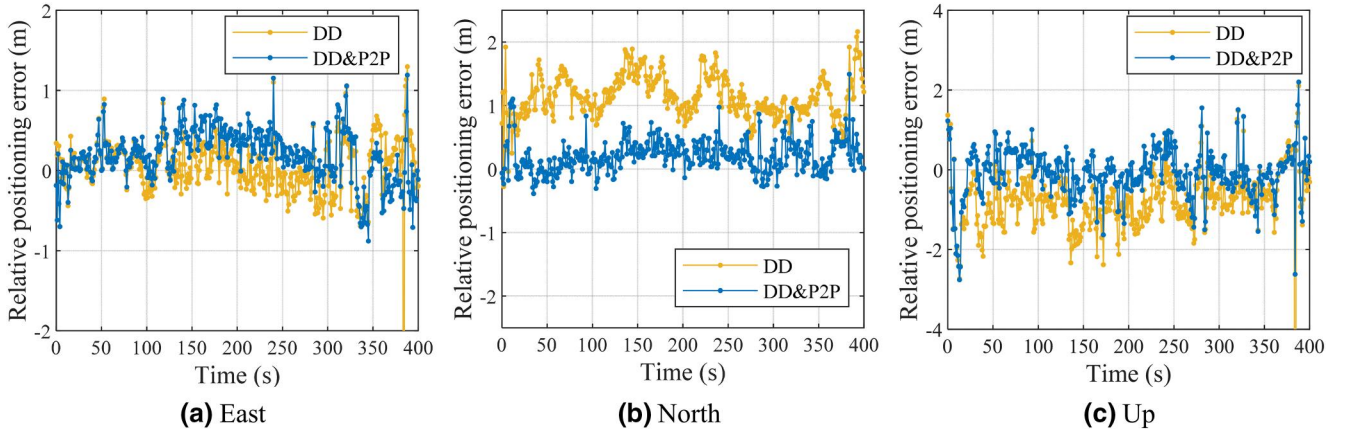


FIGURE 20 The relative positioning error comparison between the two relative navigation methods (DD and DD&P2P)

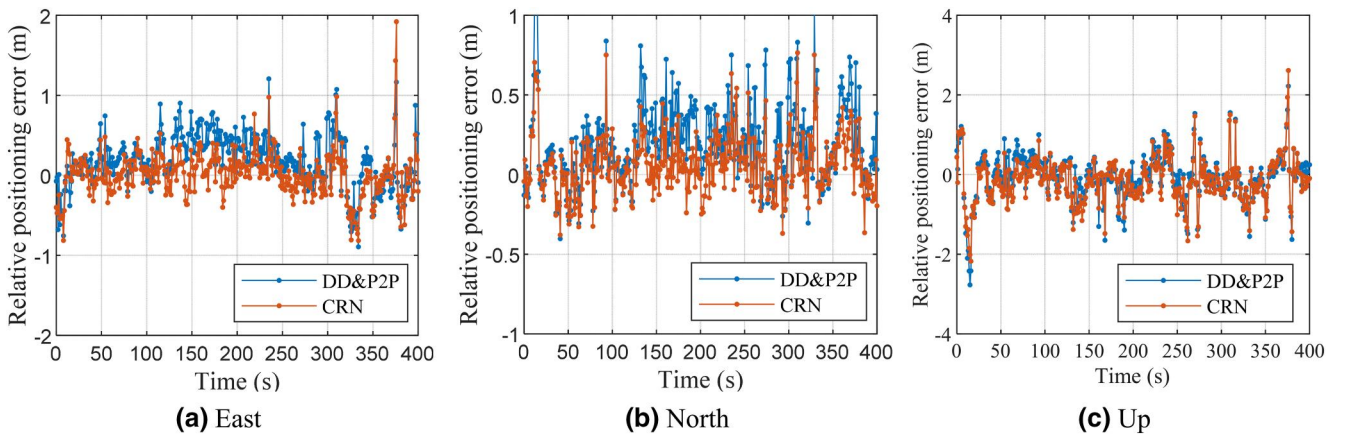


FIGURE 21 The relative positioning error comparison between the two relative navigation methods (DD&P2P and CRN)

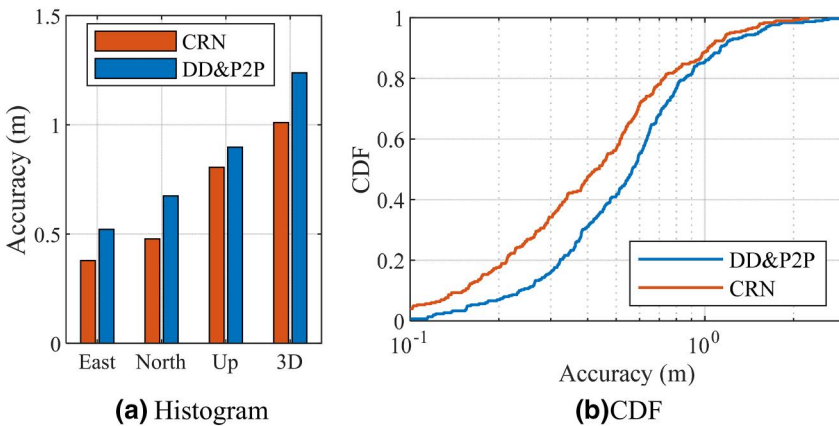


FIGURE 22 Accuracy of the baseline comparison between the two relative navigation methods with and without cooperation in the forms of (a) histogram and (b) cumulative distribution function

Then, we compare the relative navigation accuracy between the DD&P2P method and the CRN approach with Figure 21 presenting the results. As seen, the relative positioning error is reduced further by CRN method. Since the relative positioning solutions estimated by DD&P2P and CRN are close, it is not easy to distinguish from RTK on the scatter plot. Therefore, the RMS value is discussed in the histogram, as shown in Figure 22(a). The comparison results indicate that

the cooperation of multiple UAVs reduces the relative positioning error from 1.24 to 1.01 m, and the performance is improved by 18.55%. The relative positioning error is below 0.5 m in the E and N directions. In addition, the CDF graph analysis is performed according to the data results, as shown in Figure 22(b).

The multi-UAV platform flight experiment verifies the algorithm with real data and reflects the effective improvement

of the relative navigation performance of the multi-UAV formation by the proposed cooperative relative navigation algorithm.

## 5 | CONCLUSION AND FUTURE WORK

We propose a cooperative relative navigation algorithm for multi-UAV systems based on GNSS and P2P ranging measurements. Simulations and experiments demonstrate that employing P2P ranging measurements to assist the traditional DD pseudorange can effectively improve the navigation accuracy, especially under GNSS challenging scenarios. In addition, the performance of relative navigation can be further improved by cooperating the information from other UAVs in the formation, which builds a cooperative relative navigation technology. Sensitivity analyses suggest that the performance is highly dependent on the formation geometry, the formation scale, and the accuracy of the P2P ranging measurements. And these influencing factors have been quantitatively addressed in the results.

The future work includes (a) conducting performance evaluation with more realistic error models, (b) designing a cooperative FDE scheme to account for large errors caused by heavy multipath interference and NLOS reception, and (c) employing other sensors, such as barometer, IMU and vision.

## ACKNOWLEDGEMENTS

This work is supported by Key R&D Program Projects in Jiangxi Province: Key Technologies of Intelligent High-speed Application Service Based on Beidou System (NO. 20181ACE50027) and 5G Telecommunication Project in Jiangxi Province: Research on Free Flow Toll Collection Technology Based on 5G + Beidou System (NO. 20193ABC03A006). This work is also supported by the Research Achievements Industrialization Foundation of the MoE Research Center on Aerospace Science and Technology.

## ORCID

Shizhuang Wang  <https://orcid.org/0000-0003-3518-2281>

Yawei Zhai  <https://orcid.org/0000-0002-6552-5903>

Xingqun Zhan  <https://orcid.org/0000-0002-7655-067X>

## REFERENCES

- Valavanis, K.P., Vachtsevanos, G.J.: Handbook of Unmanned Aerial Vehicles. Springer Press (2014).
- Rufa, J.R., Atkins, E.M.: Unmanned Aircraft system navigation in the urban environment: a systems analysis. *J. Aerosp. Infor. Syst.* 12(12), 143–160 (2016)
- Shakhathreh, H., et al.: Unmanned aerial vehicles (UAVs): a survey on civil applications and key research challenges. *IEEE Access.* 7, 48572–48634 (2019)
- Safwat, N.E., Newagy, F., Hafez, I.M.: Air-to-ground channel model for UAVs in dense urban environments. *IET Commun.* 14(6), 1016–1021 (2020)
- Chung, S., et al.: A survey on aerial swarm robotics. *IEEE Trans. Robot. Autom.* 34(4), 837–855 (2018)
- Shen, F., Cheong, J., Dempster, A.: A DSRC Doppler/IMU/GNSS tightly-coupled cooperative positioning method for relative positioning in VANETs. *J. Navig.* 70(1), 120–136 (2017)
- Li, W., et al.: Adaptive robust Kalman filter for relative navigation using global position system. *IET Radar Sonar Navig.* 7(5), 471–479 (2013)
- Chen, M., et al.: Localisation-based autonomous vehicle rear-end collision avoidance by emergency steering. *IET Intell. Transp. Syst.* 13(7), 1078–1087 (2019)
- Ko, H., Kim, B., Kong, S.: GNSS multipath-resistant cooperative navigation in urban vehicular networks. *IEEE Trans. Veh. Technol.* 64(12), 5450–5463 (2015)
- Su, X., et al.: Receiver autonomous integrity monitoring (RAIM) performances of combined GPS/BeiDou/QZSS in urban canyon. *IEE J. Trans. Electr. Electron. Eng.* 9(3), 275–281 (2014)
- Tabatabaei, A., Mosavi, M.R.: Robust adaptive joint tracking of GNSS signal code phases in urban canyons. *IET Radar Sonar Navig.* 11(6), 987–993 (2017)
- Saeed, A.S., et al.: A review on the platform design, dynamic modeling and control of hybrid UAVs. In: 2015 International Conference on Unmanned Aircraft Systems (ICUAS), pp. 806–815. Denver, CO (2015)
- Haken, H: Synergetics. Springer-Verlag Press, Berlin (1977)
- Ferri, G., et al.: Cooperative robotic networks for underwater surveillance: an overview. *IET Radar Sonar Navig.* 11(12), 1740–1761 (2017)
- Hu, Y., et al.: Placement optimisation method for multi-UAV relay communication. *IET Commun.* 14(6), 1005–1015 (2020)
- Tahir, M., et al.: On the accuracy of inter-vehicular range measurements using GNSS observables in a cooperative framework. *IEEE Trans. Intell. Transp. Syst.* 20(2), 682–691 (2019)
- Ducatelle, F., et al.: Cooperative navigation in robotic swarms. *Swarm Intell.* 8(1), 1–33 (2014)
- Roumeliotis, S.I., Bekey, G.A.: Distributed multi-robot localization. *IEEE Trans. Robot. Autom.* 18, 781–795 (Oct. 2002)
- Mourikis, A.I., Roumeliotis, S.I.: Performance analysis of multi-robot cooperative localization. *IEEE Trans. Robot.* 22, 666–681 (2006)
- Sivaneri, V.O., Gross, J.N.: UGV-to-UAV cooperative ranging for robust navigation in GNSS-challenged environments. *Aero. Sci. Technol.* 71, 245–255 (2017)
- Causa, F., et al.: Multi-UAV formation geometries for cooperative navigation in GNSS-challenging environments. In: 2018 IEEE/ION Position, Location and Navigation Symposium (PLANS), pp. 775–785. Monterey, CA (2018)
- Wang, X., Cui, N., Guo, J.: INS/VisNav/GPS relative navigation system for UAV. *Aero. Sci. Technol.* 28(1), 242–248 (2013)
- Walter, V., et al.: UVDAR system for visual relative localization with application to leader–follower formations of multirotor UAVs. *IEEE Robot. Autom. Lett.* 4(3), 2637–2644 (2019)
- Strader, J., et al.: Cooperative relative localization for moving UAVs with single link range measurements. In: 2016 IEEE/ION Position, Location and Navigation Symposium (PLANS), pp. 336–343. Savannah, GA (2016)
- Gross, J.N., Gu, Y., Rhudy, M.B.: Robust UAV relative navigation with DGPS, INS, and peer-to-peer radio ranging. *IEEE Trans. Autom. Sci. Eng.* 12(3), 935–944 (2015)
- Xiong, J., et al.: Close relative navigation algorithm for unmanned aerial vehicle aided by UWB relative measurement. *J. Chin. Inert. Technol.* (in Chinese). 26(03), 346–351 (2018)
- Nguyen, T., et al.: Distance-based cooperative relative localization for leader-following control of MAVs. *IEEE Robot. Autom. Lett.* 4(4), 3641–3648 (2019)
- Guo, K., Li, X., Xie, L.: Ultra-wideband and odometry-based cooperative relative localization with application to multi-UAV formation control. *IEEE Trans. Cybernet.* 50(6), 2590–2603 (2020)
- She, F., et al.: Enhanced relative localization based on persistent excitation for multi-UAVs in GPS-denied environments. *IEEE Access.* 8, 148136–148148 (2020)
- Wang, Y., Chen, X., Liu, P.: Statistical multipath model based on experimental GNSS data in static urban canyon environment. *Sensors.* 18, 1149 (2018)

31. Elliott, K., Hegarty, C.: *Understand GPS/GNSS: Principles and Applications*, 3rd ed. Artech Press, Norwood, MA (2017)
32. Müller, F.P., et al.: Bayesian cooperative relative vehicle positioning using pseudorange differences. In: *2014 IEEE/ION Position, Location and Navigation Symposium*, pp. 434–444. Monterey, CA (2014)
33. Wang, S., et al.: Highly reliable relative navigation for multi-uav formation flight in urban environments. *Chin. J. Aeronaut.* Online Access. (2020). <https://doi.org/10.1016/j.cja.2020.05.022>
34. Salós, D., et al.: Nominal GNSS pseudorange measurement model for vehicular urban applications. In: *IEEE/ION Position, Location and Navigation Symposium*, pp. 806–815. Wells, CA (2010)
35. Blanch, J., et al.: Baseline advanced RAIM user algorithm and possible improvements. *IEEE Trans. Aero. Electron. Syst.* 51, 713–732 (2015)
36. Jeffrey, C.: *An Introduction to GNSS: GPS, GLONASS, BeiDou, Galileo and other Global Navigation Satellite Systems*, 2nd ed. NovAtel Inc. Press (2015)
37. Hsu, L.T., et al.: Multiple faulty GNSS measurement exclusion based on consistency check in urban canyons. *IEEE Sensor J.* 17(6), 1909–1917 (2017)
38. RTKLIB ver. 2.4.2 manual, <http://www.rtklib.com/>
39. Luo, J.L., Mo, B., Lin, J.: A design of high-precision positioning system of UAV based on the Qianxun location network. In: *Proceedings of 37th Chinese Control Conference (CCC)*, pp. 4633–4637. Wuhan, China (2018)

**How to cite this article:** Shen J, Wang S, Zhai Y, Zhan X. Cooperative relative navigation for multi-UAV systems by exploiting GNSS and peer-to-peer ranging measurements. *IET Radar Sonar Navig.* 2020;1–16. <https://doi.org/10.1049/rsn2.12023>